17p

NASA TR R-146

N63-14972
Code-1

NATIONAL AERONAUTICS AND SPACE ADMINISTRATION

TECHNICAL REPORT
R-146

LAMINAR BOUNDARY-LAYER SEPARATION INDUCED BY FLARES ON CYLINDERS AT ZERO ANGLE OF ATTACK

By DONALD M. KUEHN

1962

24p 554226

For sale by the Superintendent of Documents, U.S. Government Printing Office, Washington 25, D.C. Yearly subscription, $15: foreign, $19; single copy price varies according to size. ---------- Price 30 cents

TECHNICAL REPORT R-146

LAMINAR BOUNDARY-LAYER SEPARATION INDUCED BY FLARES ON CYLINDERS AT ZERO ANGLE OF ATTACK

By DONALD M. KUEHN

Ames Research Center
Moffett Field, Calif.

TECHNICAL REPORT R-146

LAMINAR BOUNDARY-LAYER SEPARATION INDUCED BY FLARES ON CYLINDERS AT ZERO ANGLE OF ATTACK

By DONALD M. KUEHN

SUMMARY

14972

Laminar boundary-layer separation induced by conical flares on cylindrical bodies of revolution has been experimentally investigated in the Mach number range of 2.0 to 5.5 at Reynolds numbers, based on boundary-layer thickness, from 1×10^5 to 30×10^5. Geometric variables were nose shape, cylinder length, and flare angle, and test variables were Mach number, Reynolds number, and heat transfer. The purpose of the investigation was to determine which of these variables most influence laminar boundary-layer separation on cylinder-flare configurations and to provide data that will aid in the prediction of laminar separation.

The results showed that the tendency toward laminar separation decreased as Mach number or heat transfer to the model was increased and as Reynolds number or flare angle was decreased. Cylinder length and nose shape had no influence on the variation of Mach number for incipient separation with Reynolds number based upon boundary-layer thickness. Conditions for incipient separation on blunt- and sharp-nosed cylinders correlated whether determined from properties in the free stream or at the model surface.

INTRODUCTION

It is important that the occurrence of boundary-layer separation be predictable since separation can alter heat transfer, pressure distribution, and the over-all forces and moments on aircraft, missiles, and entry vehicles. This point is discussed in reference 1 in which data were presented for flare-stabilized bodies of revolution having turbulent boundary layers. As flight trajectories extend to higher altitudes, however, the laminar boundary layer becomes more prevalent and thus information is also required on the occurrence of laminar separation. The purpose of the present investigation is to determine some of the variables that are important to laminar boundary-layer separation on a cylinder-flare configuration and to provide data that will aid in the prediction of laminar separation.

NOTATION

D	diameter of cylinder, in.
l	distance along the model measured from the cylinder-flare juncture, in. (minus upstream, plus downstream)
L	length of model or of model component, in.
M	Mach number (for sharp-nosed models $M_\infty=M_w$)
p	pressure, psia
R	Reynolds number, $\frac{u\delta_0}{12\nu}$ (for sharp-nosed models $R_{\infty\delta_0}=R_{w\delta_0}$)
S	approximate location of the separation point
u	velocity, ft/sec
x	distance along model axis measured from the nose-cylinder juncture, in.
y	distance from model normal to the surface, in.
δ	boundary-layer thickness, in.
θ	flare angle, deg
μ	viscosity, lb sec/ft^2
ν	kinematic viscosity, $\frac{\mu}{\rho}$, ft^2/sec
ρ	density, lb sec^2/ft^4

SUBSCRIPTS

cyl	cylindrical section of the model
flare	flared portion of the model
incip	incipient separation
w	inviscid condition at the wall (body surface)
∞	free stream
0	location on the cylinder where the static pressure is first affected by the presence of the flare
probe	quantity determined from measurements made with the boundary-layer probe

APPARATUS AND TEST METHODS

TEST FACILITY

The tests were conducted in the Ames 1- by 3-Foot Supersonic Wind Tunnel which is a continuous-operation, closed-circuit tunnel. The minimum supersonic Mach number is about 1.2 to 1.6 and the maximum is about 5.0 to 6.0, depending on the size of the model. The maximum range of free-stream Reynolds number is approximately 3×10^5 to 9×10^6 per foot. The Mach number and free-stream Reynolds number are continuously variable during tunnel operation.

MODELS AND MEASUREMENTS

The models used to study the occurrence of separation were cylindrical bodies of revolution with flared afterbodies, sting mounted at zero angle of attack. The geometric variables were cylinder length, nose shape, and flare angle. The shape of both the pressure-distribution and the heat-transfer models and the model designations are presented in figure 1. The model for evaluating the influence of heat transfer on the occurrence of separation was constructed of solid aluminum and was mounted on an insulated sting.

Longitudinal surface-pressure distributions, boundary-layer surveys, and shadowgraphs of the flow field were obtained to determine the presence of boundary-layer separation. The detection of separation by means of boundary-layer surveys was a tedious process, thus this method was not used extensively. The shadowgraphs clearly showed large regions of separation, but generally the pressure distribution was the only satisfactory means for detecting the presence of very small separated regions. More will be said later on detection of separation. The static pressures were measured with differential-type pressure

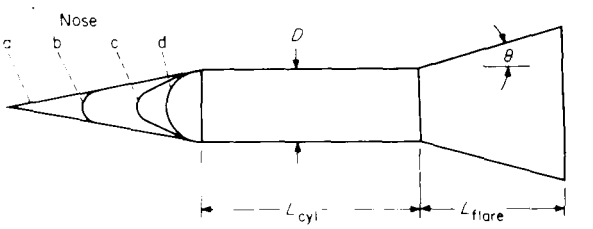

Nose a sharp cone; 20° included angle
b blunted cone; 20° included angle; nose radius = $D/4$
c blunted cone; 45° included angle; nose radius = $D/4$
d hemisphere

Pressure-distribution model ($D=1.25$ in.)
$L_{cyl}/D=1.0, 2.6, 4.2$
$\theta=5.0, 7.5, 10.0$
$L_{flare}/D=2.5$
Noses a, b, c, d

Heat-transfer model ($D=0.50$ in.)
$L_{cyl}/D=1.0, 2.0$
$\theta=15, 20$
$L_{flare}/D=2.5$
Noses a, b, c, d

Example designation: CC5–b–2.6
L_{cyl}/D
Compression-corner flare, $\theta=5°$
Nose geometry

FIGURE 1.—Model geometry and designations.

cells to an approximate accuracy of 0.004 psi. The shape of the pressure-distribution curves was, however, determined more accurately than indicated by this absolute error because a portion of the 0.004 psi error was such that the measured pressure-distribution curve was displaced from the true curve but was parallel to it.

Heat-transfer models were used to evaluate qualitatively the influence of heat flow into the model surface. The model was enclosed with a shroud, and liquid nitrogen was circulated around the model until the desired temperature was attained. The shroud was then removed and a temperature record and shadowgraphs were obtained. Only shadowgraphs were used to study the occurrence of separation on the heat-transfer models.

Model instrumentation included static pressure orifices for pressure measurement and thermocouples for temperature measurement. The pressure-distribution model had 0.0135-inch-diameter orifices extending from 0.8 D ahead of the flare

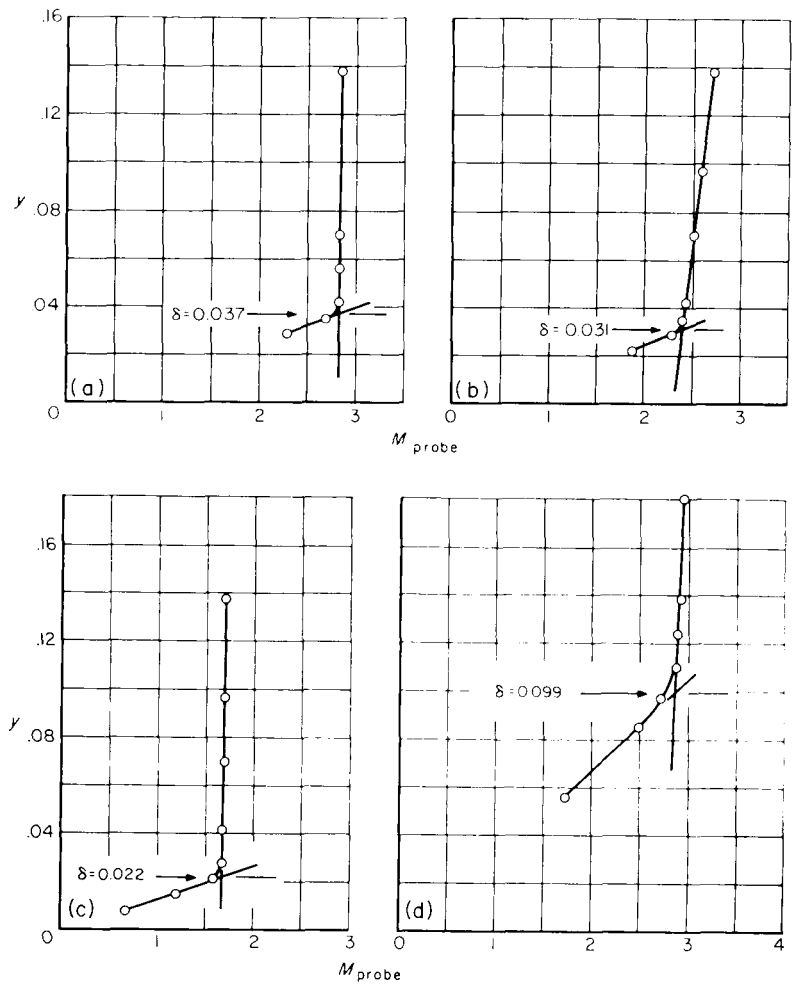

(a) 20° sharp conical nose; $M_\infty = 2.92$; $R_\infty/\text{in.} = 2.5 \times 10^5$.
(b) 20° blunt conical nose; $M_\infty = 3.41$; $R_\infty/\text{in.} = 4.6 \times 10^5$.
(c) Hemispherical nose; $M_\infty = 1.90$; $R_\infty/\text{in.} = 2.0 \times 10^5$.
(d) Hemispherical nose; $M_\infty = 4.76$; $R_\infty/\text{in.} = 1.0 \times 10^5$.

FIGURE 2.—Boundary-layer thickness measurements.

on the cylinder to near the base of the flare. The longitudinal spacing of orifices was 0.04 D in regions where large pressure gradients were expected, and larger spacing in the region of smaller expected pressure gradients. The heat-transfer model was not instrumented for pressure measurement, but it contained a thermocouple near the cylinder-flare juncture.

OPTICAL EQUIPMENT

For all test conditions, the boundary layer and shock patterns were observed visually and were recorded. A continuous operation shadowgraph was used to view the flow field during the tests, and a spark shadowgraph with spark duration of about 1 microsecond was used to obtain photographic records of the flow. The mirror and the light sources were arranged so that nearly parallel light passed through the test section. A full-sized image was thus observed on a ground-glass screen mounted near the tunnel window opposite the light source. The ground-glass screen was replaced with a Polaroid-Land film pack when photographs were desired.

BOUNDARY-LAYER SURVEYS

A probe was used to obtain pitot pressure surveys in the boundary layer. The tip of the probe had an approximately elliptical cross section of about 0.007 inch in height, 0.012 inch wide.

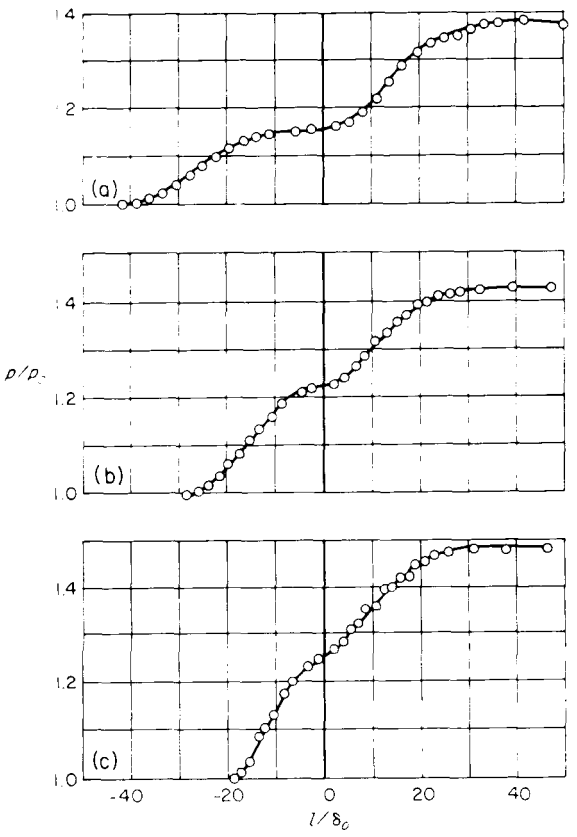

(a) $M_\infty = 1.91$; $R_{\infty\delta_0} = 7.0 \times 10^3$
(b) $M_\infty = 2.51$; $R_{\infty\delta_0} = 6.8 \times 10^3$
(c) $M_\infty = 2.92$; $R_{\infty\delta_0} = 7.4 \times 10^3$

FIGURE 3.—Longitudinal pressure distributions used to detect incipient separation; CC5-a-1.0.

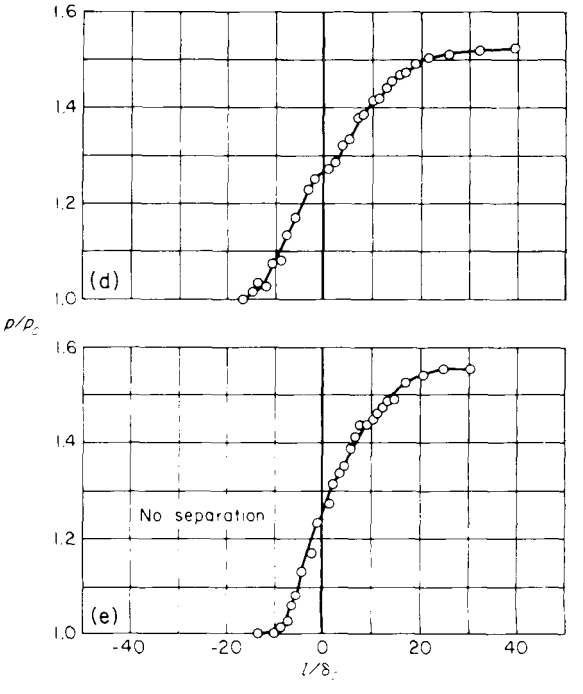

(d) $M_\infty = 3.31$; $R_{\infty\delta_0} = 7.4 \times 10^3$
(e) $M_\infty = 3.70$; $R_{\infty\delta_0} = 7.6 \times 10^3$

FIGURE 3.—Concluded.

and a 0.002-inch wall thickness. During a survey the probe was moved perpendicular to the model surface and its position relative to the surface was indicated by a counter reading obtained from a previous calibration. The probe tip could be positioned at any desired longitudinal station on the body.

Boundary-layer profiles were obtained on all nose-cylinder combinations with a flare angle of zero, except the heat-transfer model. The boundary-layer thickness thus determined at stations on the cylinder just upstream of the initial pressure rise associated with the flare is, therefore, free of flare interference. Mach number profiles were determined from the ratio of local static pressure on the model to the pitot pressure. The approximate boundary-layer thickness was determined from plots of M_{probe} versus y as shown in figure 2. For one case, discussed in the following section, profile surveys were made at several Mach numbers on a flared model at the cylinder-flare juncture.

METHOD OF DETECTING THE PRESENCE OF A SEPARATED BOUNDARY LAYER

Longitudinal pressure distributions provided the primary evidence for the existence of separated flow. Separation of the boundary layer was associated with a hump in the longitudinal pressure distribution (i.e., a pressure-distribution curve with three inflection points). The first appearance of the hump was, therefore, used as a criterion for identifying the conditions for incipient separation. This method was used in the tests reported in reference 1 for detecting the presence of turbulent separation, and is equally applicable to laminar separation. Pressure distributions are shown in figure 3 which illustrate the variation in extent of separated region with Mach number. Incipient separation is indicated at a Mach number between 3.3 and 3.7.

Boundary-layer profiles supported the evidence that the detection of separation by longitudinal pressure distribution is valid. Boundary-layer surveys were obtained at the cylinder-flare

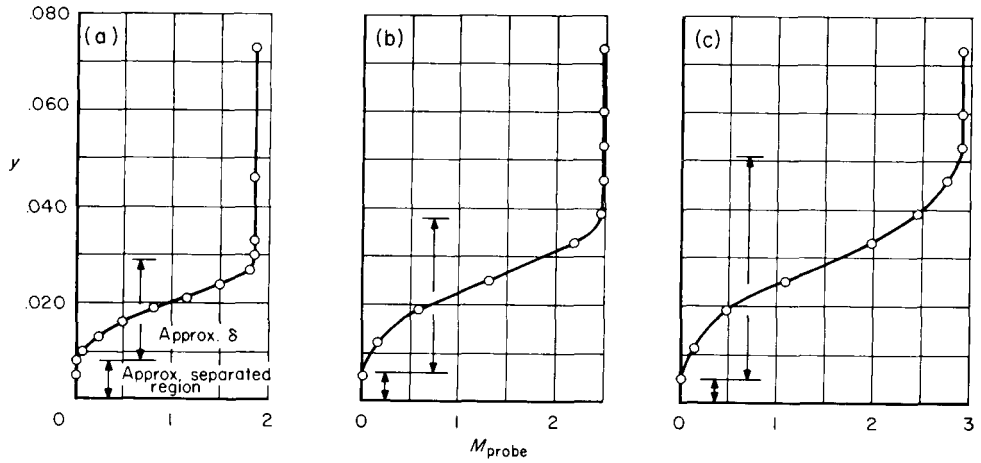

(a) $M_\infty = 1.91$; $R_{\infty \delta_0} = 7.0 \times 10^3$ (b) $M_\infty = 2.51$; $R_{\infty \delta_0} = 6.8 \times 10^3$ (c) $M_\infty = 2.92$; $R_{\infty \delta_0} = 7.4 \times 10^3$

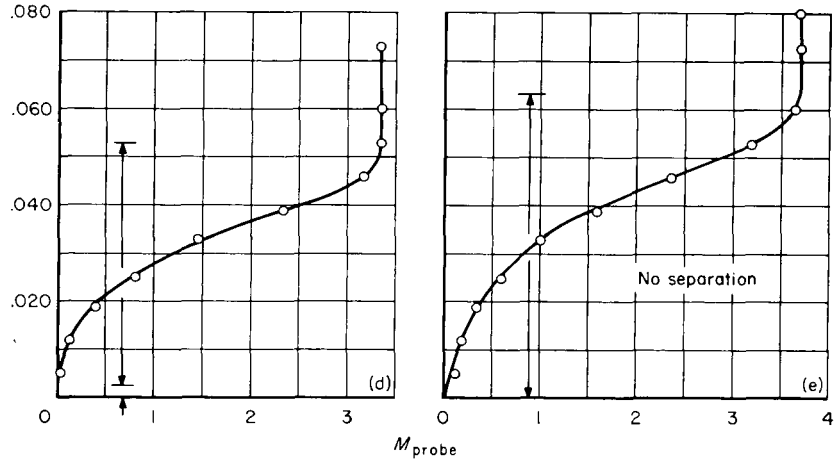

(d) $M_\infty = 3.31$; $R_{\infty \delta_0} = 7.4 \times 10^3$ (e) $M_\infty = 3.70$; $R_{\infty \delta_0} = 7.6 \times 10^3$

FIGURE 4.—Mach number profiles through the boundary layer at the cylinder-flare juncture; CC5–a–1.0.

juncture for the model and test conditions of figure 3. These surveys are shown in figure 4. The first occurrence of separation detected by the boundary-layer surveys agrees with that determined from the longitudinal pressure distribution.

Shadowgraphs were used to indicate the presence of large separated regions only since this method was not sufficiently sensitive to detect incipient separation. The flow-field details which were observed in the shadowgraphs are illustrated schematically in figure 5. Due to the very low stream density many shadowgraphs do not show these details with sufficient clarity to survive reproduction in a report. A few selected shadowgraphs of the flow about various models at conditions for which separation occurred are, therefore, shown in figure 6 to illustrate these details. Pressure distributions accompany some of the shadowgraphs.

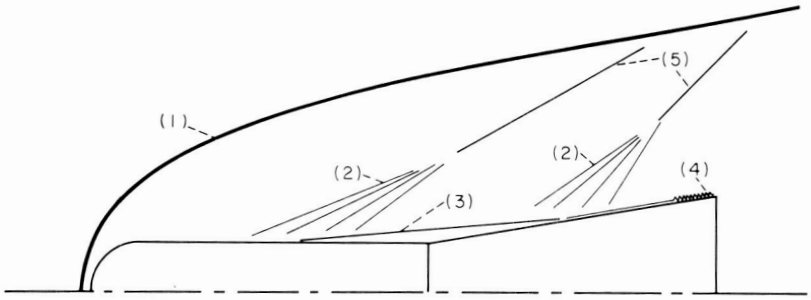

(1) Bow shock.
(2) Weak shocks produced by gradual turning of the boundary layer; these shocks not visible in shadowgraphs.
(3) White line, which represents the boundary layer, is the focal point of the light rays passing through the boundary layer (NACA Rep. 1356, 1958).
(4) Transition location—generally off the model.
(5) Strong shocks resulting from the coalescence of weak shocks, 2, from the separation and reattachment regions, respectively.

FIGURE 5.—Schematic diagram of the flow-field details observed in shadowgraphs.

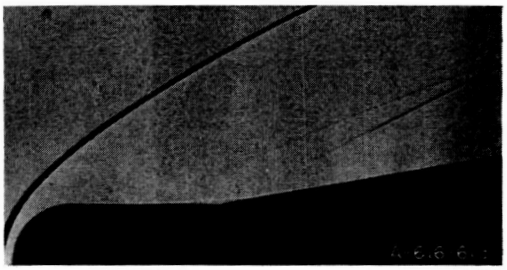

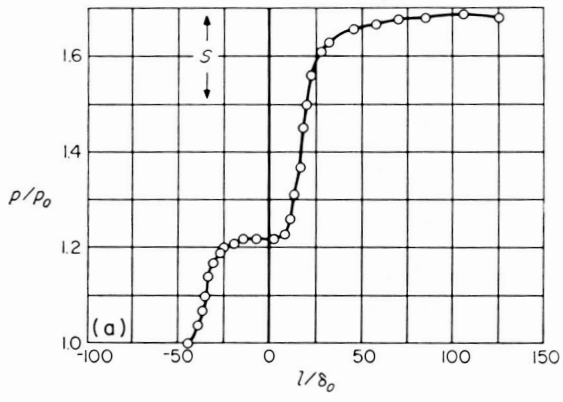

(a) CC10–d–1; $M_\infty = 2.94$; $R_{\infty\delta_0} = 6.6 \times 10^3$

FIGURE 6.—Typical pressure distributions and shadowgraphs of the flow for various model geometries.

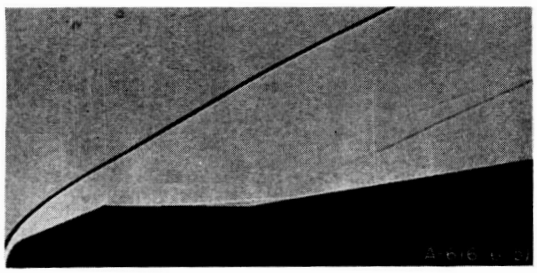

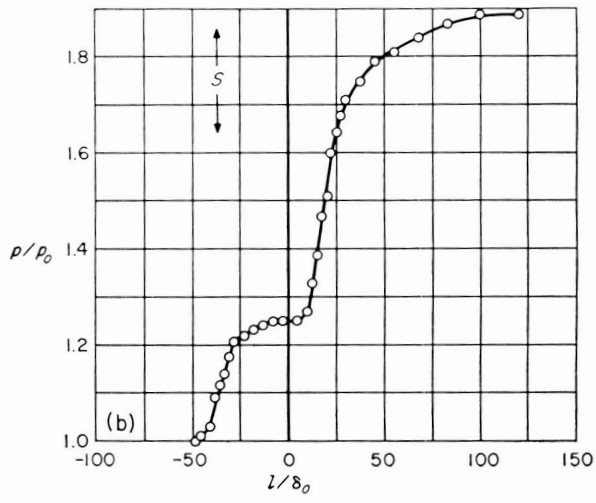

(b) CC10–c–1; $M_\infty = 2.94$; $R_{\infty\delta_0} = 4.9 \times 10^3$

FIGURE 6.—Continued.

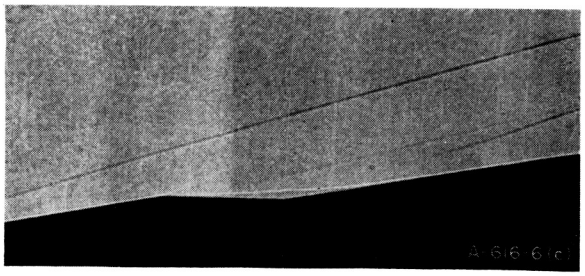

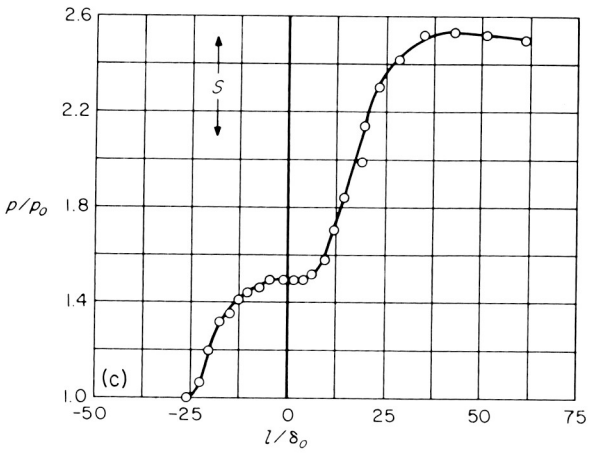

(c) CC10-a-1; $M_\infty = 4.42$; $R_{\infty \delta_0} = 11.3 \times 10^3$

FIGURE 6.—Continued.

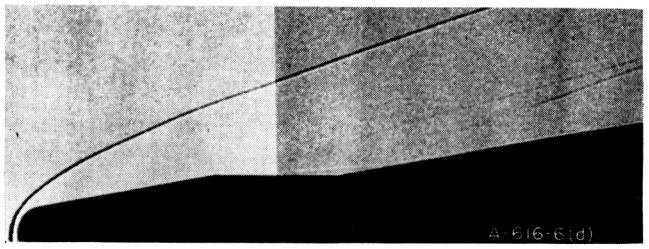

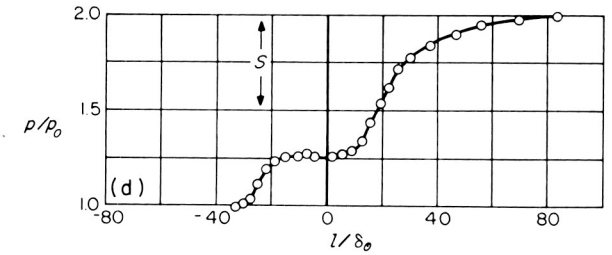

(d) CC10-b-1; $M_\infty = 3.89$; $R_{\infty \delta_0} = 10.9 \times 10^3$

FIGURE 6.—Continued.

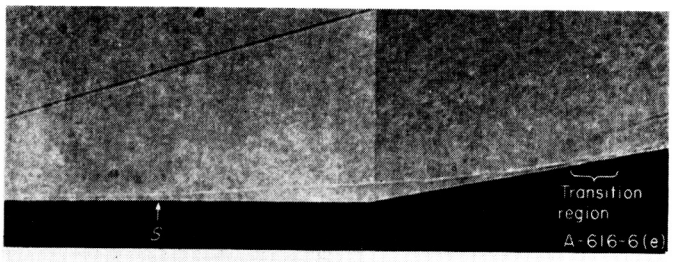

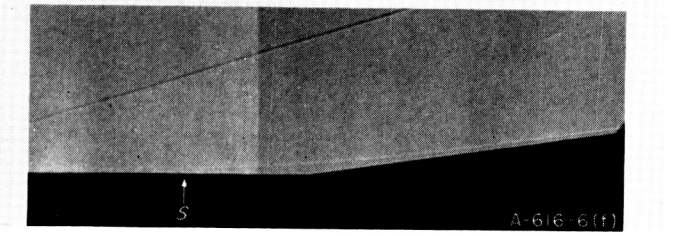

(e) CC10-a-4.2; $M_\infty = 4.75$; $R_{\infty \delta_0} = 16.7 \times 10^3$

(f) CC7.5-a-2.6; $M_\infty = 4.75$; $R_{\infty \delta_0} = 15.5 \times 10^3$

FIGURE 6.—Concluded.

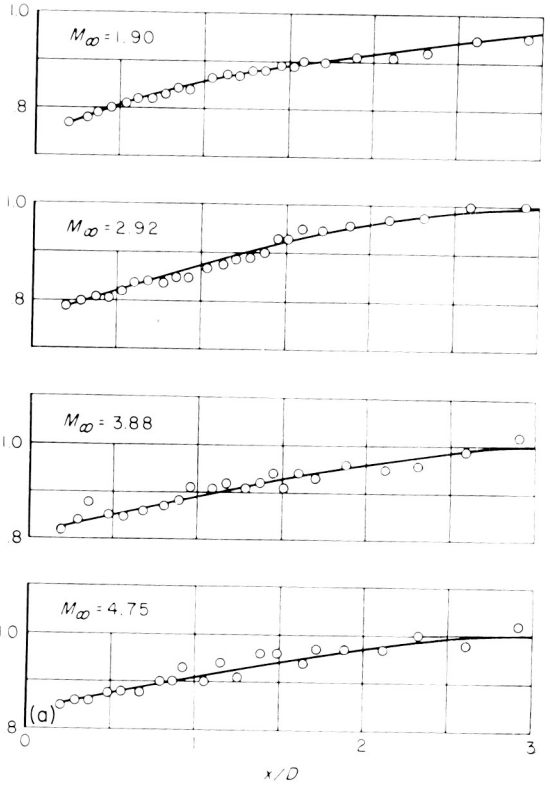

(a) 20° sharp conical nose.

FIGURE 7.—Nose-induced pressure distribution on a cylinder with no flare for each nose geometry.

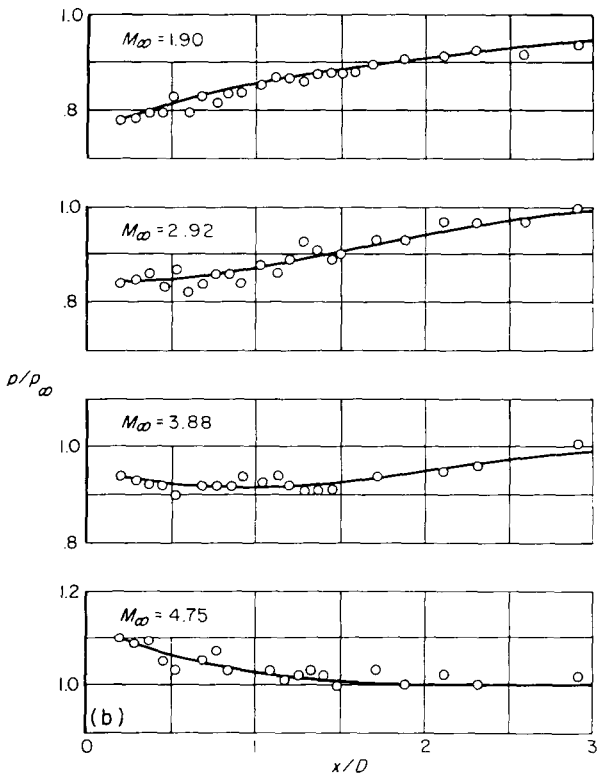

(b) 20° blunt conical nose.

FIGURE 7.—Continued.

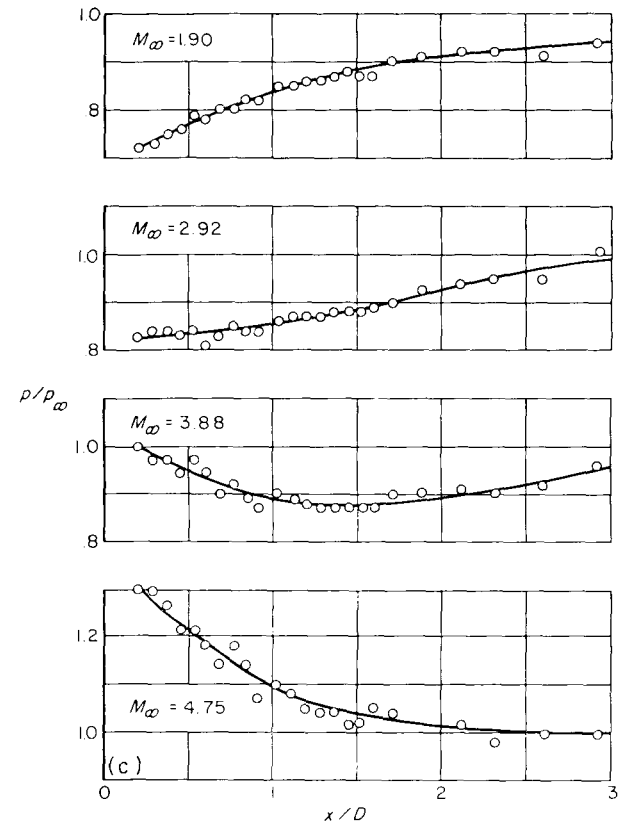

(c) 45° blunt conical nose.

FIGURE 7.—Continued.

RESULTS AND DISCUSSION

Pressure distributions on the cylinder-flare configurations result from nose-induced and flare-induced pressures. As can be seen by the nose-induced pressures in figure 7, the pressure distribution on the flare of the shortest model (flare located at $x/D=1$) will be substantially altered by the influence of the nose. The observed pressure distribution on the flare for these short models will, therefore, depend on nose shape and cylinder length as well as on Mach number and flare angle.

A boundary layer will separate from the surface when sufficient momentum has been extracted by adverse pressure gradients. For the turbulent boundary layers studied in reference 1, the adverse pressure gradient at the flare was considered to be the significant quantity responsible for the occurrence of separation because the large rate of mixing associated with a turbulent layer tends to subdue the importance of previous boundary-layer history. In contrast it is reasonable to assume that the entire pressure-gradient history of the boundary layer is important to the occurrence of laminar separation because mixing is negligible. To avoid the necessity of delving into the entire pressure-gradient history of the laminar boundary layer, the Mach number for incipient separation will be presented for given body shapes rather than for a specified pressure rise. This type of presentation evaluates the integrated influence on the separation of a laminar boundary layer of all favorable and adverse pressure gradients over the entire nose-cylinder-flare configuration.

When Mach number for incipient separation ($M_{\text{inc}_{\text{ip}}}$) is correlated as a function of Reynolds number based on boundary-layer thickness (R_{δ_0}), the flare angle is the only geometric variable of those investigated which was found to affect the

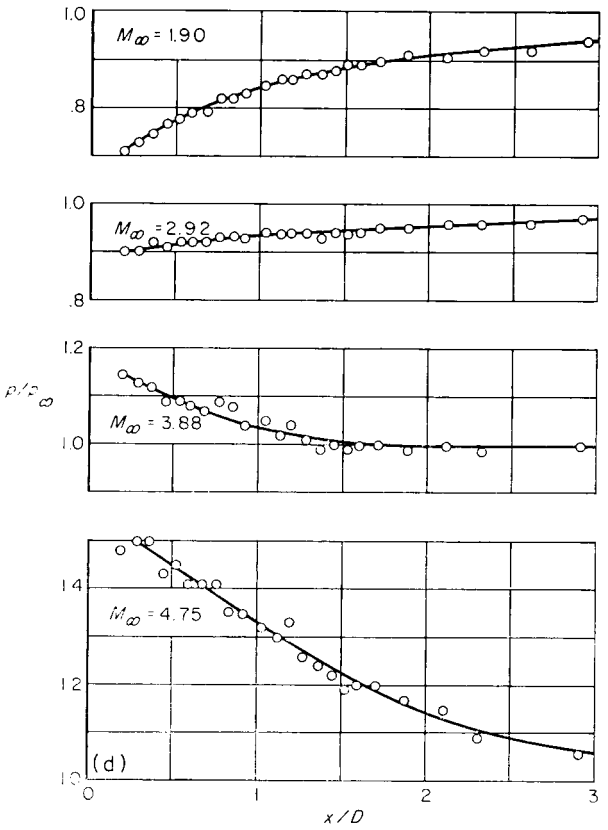

(d) Hemispherical nose.

FIGURE 7.—Concluded.

first occurrence of separation. The conditions for incipient separation determined from the longitudinal pressure distributions are shown in figures 8 and 9. Mach number at which separation is incipient is given as a function of Reynolds number for various nose geometries, flare angles, and cylinder lengths. Results are presented in terms of Mach number and Reynolds number based on free-stream values as well as on the inviscid values at the wall.[1] Boundary-layer separation exists for conditions below these curves. Above the curves the boundary layer is always attached. A separated region will appear and grow continuously if Mach number is decreased below the limit for incipient separation and vice versa. All data obtained show that the occurrence of separation depends on Reynolds number. Figures 8(a) through 8(e) show comparisons of various nose geometries and, in addition, figures 8(d) and 8(e) show comparisons of three cylinder lengths. The influences of nose shape and cylinder length evidently are effectively accounted for in boundary-layer Reynolds number since these variables had no influence on the Mach number for incipient

[1] The Mach number and Reynolds number at the wall for inviscid flow over a blunt-nosed cylinder are considerably less than the free-stream values due to the strong, detached bow wave. These wall values are computed as described in reference 2.

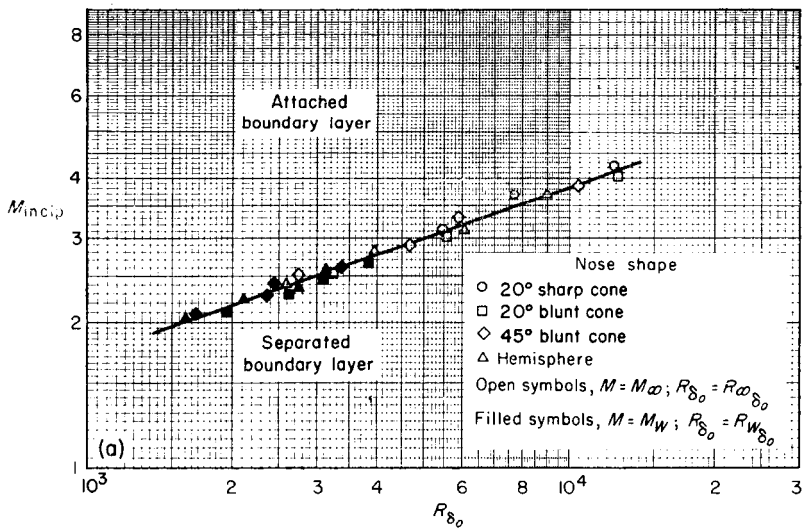

(a) $\theta = 5.0$; $(L/D)_{cyl} = 1.0$

FIGURE 8.—Conditions for the incipient separation of a laminar boundary layer on a cylinder-flare configuration.

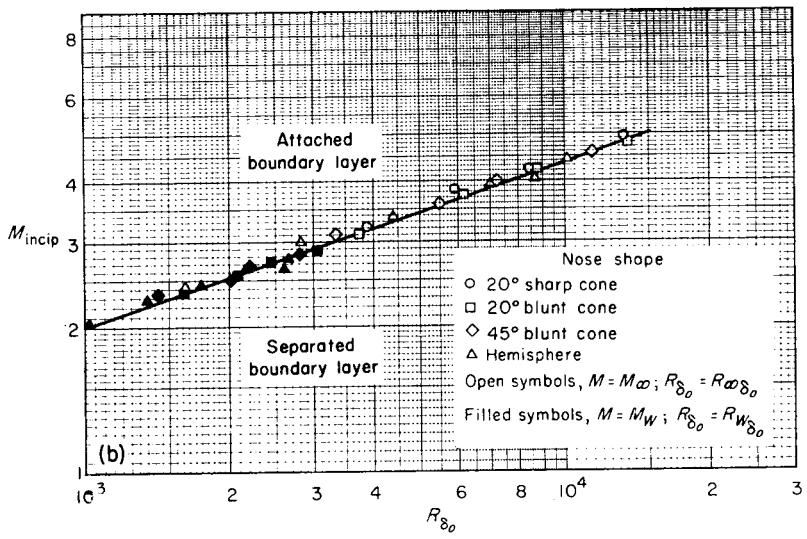

(b) $\theta = 7.5$; $(L/D)_{cyl} = 1.0$

FIGURE 8.—Continued.

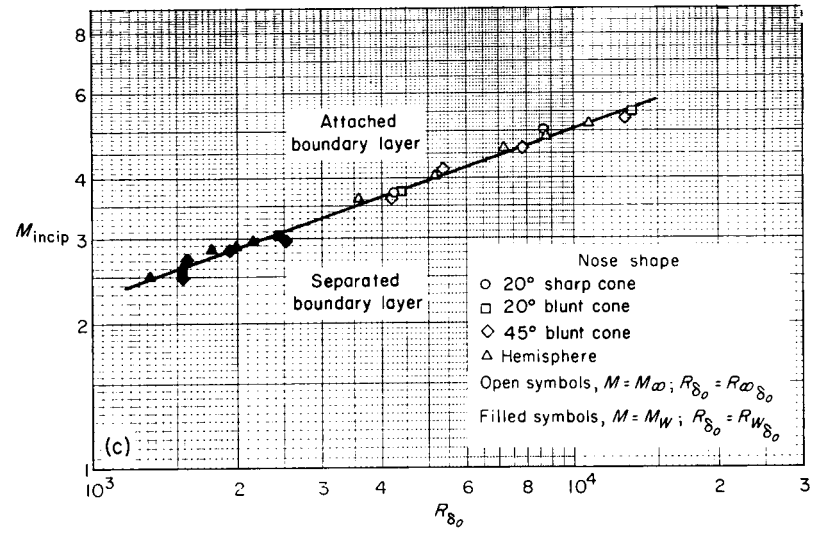

(c) $\theta = 10.0$; $(L/D)_{cyl} = 1.0$

FIGURE 8.—Continued.

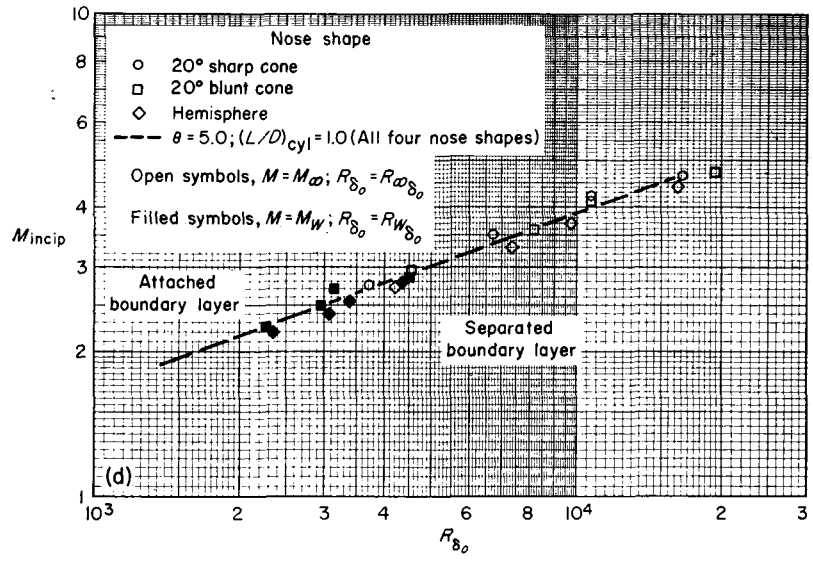

(d) $\theta = 5.0$; $(L/D)_{cyl} = 2.6$

FIGURE 8.—Continued.

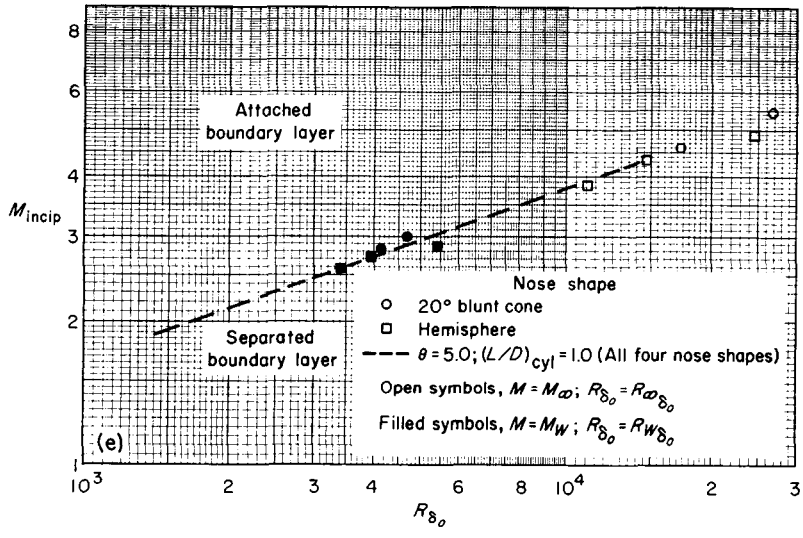

(e) $\theta = 5.0$; $(L/D)_{cyl} = 4.2$

FIGURE 8.—Concluded.

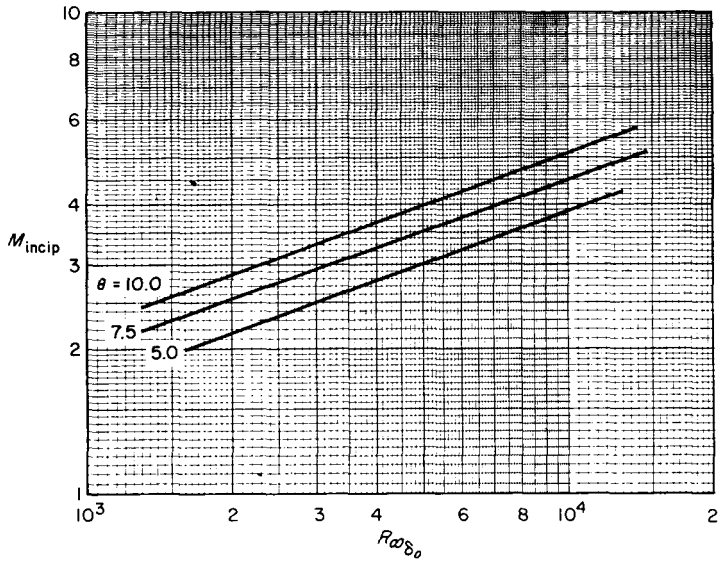

FIGURE 9.—Influence of flare angle on the conditions for incipient laminar separation.

separation when the Reynolds number was based on boundary-layer thickness. The influence of flare angle can best be seen in figure 9 which is a replot of the data in figures 8(a) through 8(c).

Although pressure distributions could not be measured on the heat-transfer models to detect separation, shadowgraphs show qualitatively that heat flow to the model decreased the extent of separation (see fig. 10). The white line, which represents the boundary layer, and the separation and reattachment shock waves were visible in the original photographs, but were difficult to distinguish in the reproductions for the report. These details were, therefore, traced with dashed lines on the bottom half of the photographs for ease of observing the effects of heat transfer. The upper half of each photograph was left untouched. Heat transfer to the model decreased the extent of separation over the entire range of Mach number and Reynolds number. This trend has been predicted in references 3 through 5 and observed experimentally in references 6 and 7.

The qualitative effects of geometry and test conditions on the occurrence of laminar separation are very similar to those found for turbulent boundary layers in reference 1. It appears that the only important difference between the laminar and turbulent boundary layers, with respect to the occurrence of separation, is that a much smaller flare angle is necessary to cause laminar separation than that necessary for turbulent separation (see fig. 11). Thus for a given model geometry, the extent of separation will be much larger for a laminar boundary layer than for a turbulent boundary layer.

CONCLUSIONS

The following conclusions result from the investigation of laminar boundary-layer separation on a cylinder-flare body of revolution in supersonic flow:

1. The tendency of the laminar boundary layer to separate decreased as Mach number was increased or as Reynolds number or flare angle was decreased.

2. The Mach number at which flare-induced boundary-layer separation first occurred at a given Reynolds number (based upon boundary-layer thickness) was not affected by changing nose shape or cylinder length.

3. The conditions for incipient separation for blunt- and sharp-nosed cylinders correlate whether determined from properties in the free stream or at the wall.

4. Heat flow into the model reduced the extent of boundary-layer separation.

AMES RESEARCH CENTER
NATIONAL AERONAUTICS AND SPACE ADMINISTRATION
MOFFETT FIELD, CALIF., *June 19, 1962*

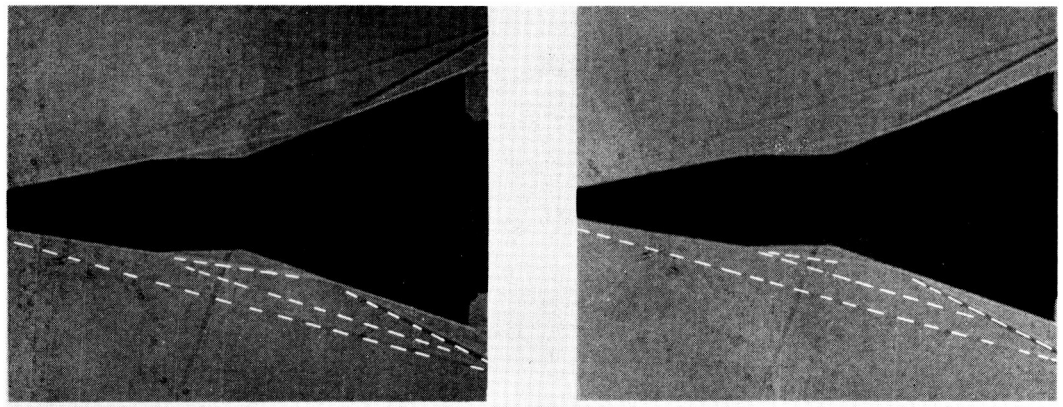

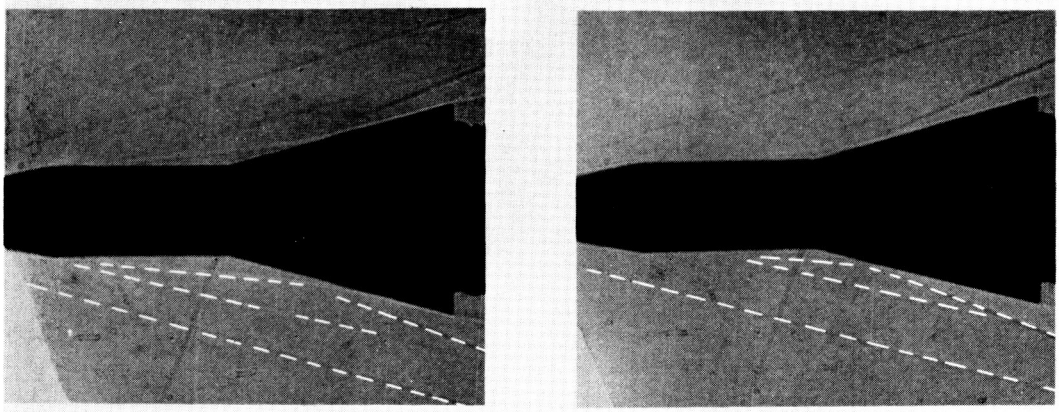

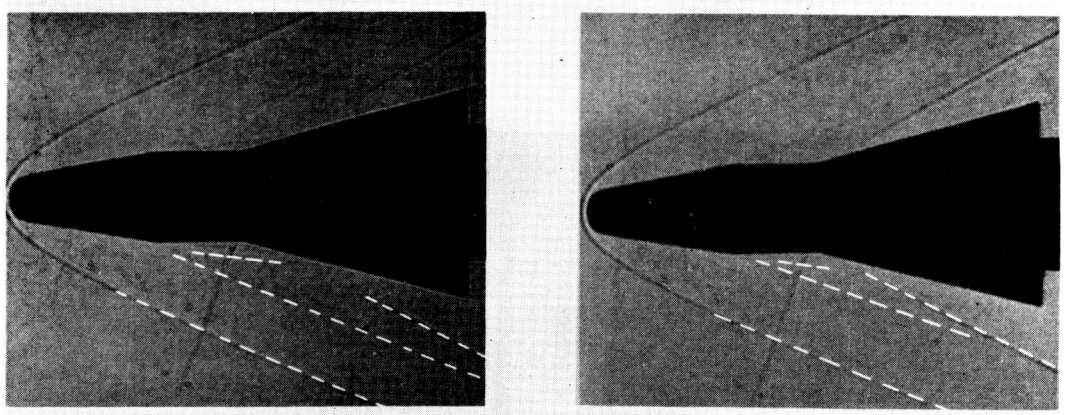

(a) CC20–a–1; $M_\infty = 4.6$; $R_\infty/\text{in.} = 2.6 \times 10^5$

(b) CC15–a–2; $M_\infty = 4.6$; $R_\infty/\text{in.} = 2.3 \times 10^5$

(c) CC15–b–1; $M_\infty = 2.9$; $R_\infty/\text{in.} = 2.0 \times 10^5$

$\frac{\text{Wall temperature}}{\text{Adiabatic wall temperature}} = 1.0$ $\qquad$ $\frac{\text{Wall temperature}}{\text{Adiabatic wall temperature}} \approx 0.38$

FIGURE 10.—Influence of heat transfer on the extent of laminar separation.

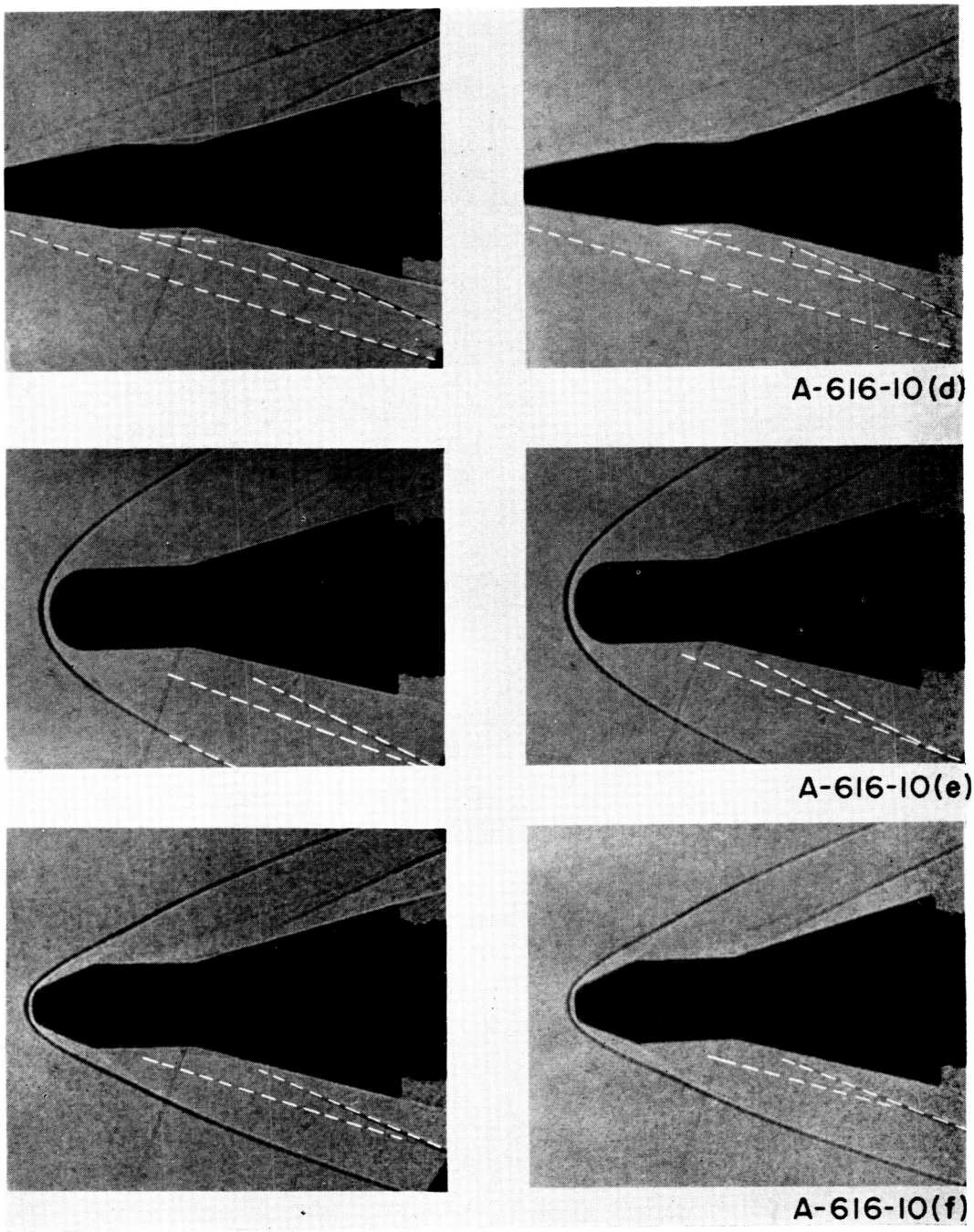

(d) CC15–a–1; $M_\infty = 3.9$; $R_\infty/\text{in.} = 3.2 \times 10^5$

(e) CC15–d–1; $M_\infty = 2.9$; $R_\infty/\text{in.} = 2.0 \times 10^5$

(f) CC15–c–1; $M_\infty = 3.9$; $R_\infty/\text{in.} = 4.3 \times 10^5$

$\frac{\text{Wall temperature}}{\text{Adiabatic wall temperature}} = 1.0$ $\frac{\text{Wall temperature}}{\text{Adiabatic wall temperature}} \approx 0.38$

FIGURE 10.—Concluded.

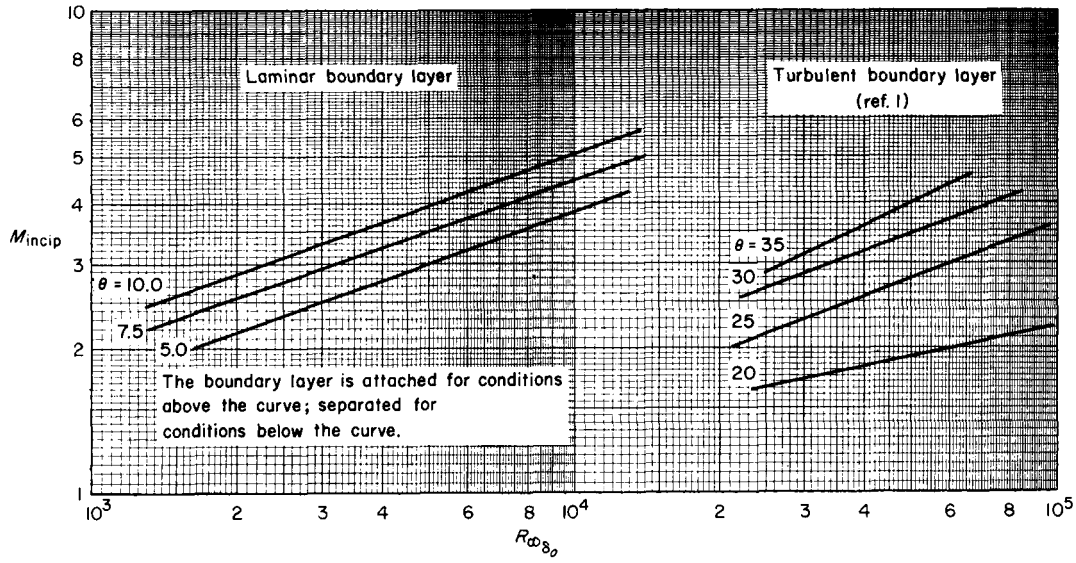

FIGURE 11.—Conditions for flare-induced separation of laminar and turbulent boundary layers.

REFERENCES

1. Kuehn, Donald M.: Turbulent Boundary-Layer Separation Induced by Flares on Cylinders at Zero Angle of Attack. NASA TR R–117, 1961.
2. Moeckel, W. E.: Some Effects of Bluntness on Boundary-Layer Transition and Heat Transfer at Supersonic Speeds. NACA Rep. 1312, 1957. (Supersedes NACA TN 3653.)
3. Curle, N.: The Effects of Heat Transfer on Laminar Boundary Layer Separation in Supersonic Flow. British ARC 21,986—F.M. 2965, 1960.
4. Gadd, G. E.: Boundary-Layer Separation in the Presence of Heat Transfer. National Physical Lab/Aero/400, British, 1960.
5. Bray, K. C., Gadd, G. E., and Woodger, M.: Some Calculations by the Crocco-Lees and Other Methods of Interactions Between Shock Waves and Laminar Boundary Layers, Including Effect of Heat Transfer and Suction. British ARC 21,834—F.M. 2937, 1960.
6. Gadd, G. E., and Attridge, J. L.: A Note on the Effects of Heat Transfer on the Separation of a Laminar Boundary Layer. British ARC 22,558—F.M. 3050, 1961.
7. Laukford, J. L.: The Effect of Heat Transfer on the Separation of Laminar Flow Over Axisymmetric Compression Surfaces—Preliminary Results at Mach Number 6.78. NAVWEPS Rep. 7402, 1961.